

# Randomness in infinitesimal extent in the McLerran-Venugopalan model

Kenji Fukushima

*Yukawa Institute for Theoretical Physics, Kyoto University, Kyoto 606-8502, Japan*

We study discrepancy between the analytical definition and the numerical implementation of the McLerran-Venugopalan (MV) model. The infinitesimal extent of a fast-moving nucleus should retain longitudinal randomness in the color source distribution even when the longitudinal extent approximates zero due to the Lorentz contraction, which is properly taken into account in the analytical treatment. We point out that the longitudinal randomness is lost in numerical simulations because of lack of the path-ordering of the Wilson line along the longitudinal direction. We quantitatively investigate how much the results with and without longitudinal randomness differ from each other. We finally mention that the discrepancy could be absorbed in a choice of the model parameter in the physical unit, and nevertheless, it is important for a full theory approach.

PACS numbers: 24.85.+p, 12.38.-t, 25.75.-q

## I. INTRODUCTION

It is a tempting idea to approximate the wavefunction of an interacting particle by mediating gauge fields surrounding the particle. Such a description of a fast-moving charged particle by virtual photons is long known as the Weizsäcker-Williams approximation. If we apply this idea to the strong interaction, we can approximately give the wavefunction of a heavy hadron by gluon fields which extend from the local color distribution inside the hadron. The formalism of the Color Glass Condensate (CGC) can accommodate the non-Abelian extension of the Weizsäcker-Williams approximation [1, 2].

The CGC formalism aims to embody the parton saturation picture arising as a result of the small- $x$  evolution at high energies [3]. The geometric scaling beautifully indicates the existence of the saturation scale as a function of Bjorken's  $x$  [4]. The CGC formalism has been forming an important building-block of Quantum Chromodynamics (QCD) at high energies. With a Gaussian approximation for distribution of the random color source and its dispersion given by the saturation scale [5], we reach the McLerran-Venugopalan (MV) model [1].

So far, the MV model has been well examined analytically in the case of a light projectile (e.g. a color dipole, a proton, etc) scattering off a dense CGC target [6, 7, 8, 9, 10, 11, 12]. The scattering problem of two CGC objects, i.e. high-energy nucleus-nucleus collision [13, 14, 15, 16, 17] is hard to solve analytically, however, and the possible analysis is limited to the numerical method [18, 19, 20, 21, 22]. Only the initial fields right after the collision (i.e. initial conditions) are analytically known in a simple form [13, 18, 23]. The initial chromo-electric and chromo-magnetic fields are thus calculable by means of the proper Gaussian average over the color source distribution [17, 21].

In this work we will address a problem that the numerical formulation of the MV model assumes a crude approximation which leads to a significant difference from the right answer. We will clarify the physical meaning to ascertain that the assumed approximation is not acceptable. The crucial point is that the formulation involves two distinct limits in the longitudinal direction; one is the vanishing extent of a nucleus and the other is the vanishing correlation length in the random color distribution. We will then quantify how much the numerical procedure turns out to underestimate the expectation value of the initial fields as compared to the analytical answer.

One might wonder if the issue to be discussed here is academic and only a technical detail, for phenomenological models are useful as long as they can fit in with empirical data. The existing numerical simulations in the MV model are, in fact, fairly consistent with experimental observations at RHIC (Relativistic Heavy-Ion Collider). We would emphasize, however, that the MV model is not a fitting model but a theoretical description based on QCD. Therefore, one should not make little of correctness checking as a theory problem.

Even though the numerical calculations underestimate the field expectation value, one might suspect that its effect is negligible from the fact that the numerical simulation agrees with RHIC experimental data. We shall see, however, that the approximation used in the numerical simulation causes a factor over 10 in the initial energy density. Such a discrepancy is not visible in the former numerical works in the MV model because the choice of the MV model parameter  $\mu$  can absorb it. All the observables scale in accord with  $\mu$  in the saturation regime, and in the numerical simulation usually,  $\mu$  is determined so as to reproduce the particle multiplicity. As a result, for instance, twice larger  $\mu$  leads to 16 times larger energy density which may compensate for the discrepancy in the dimensionless coefficient. This “posteriori reasoning” would sound fine as a phenomenological approach. The MV model is a theory, however, as we emphasized above. The essential notion of the CGC idea is that a universal description for the hadron wavefunction becomes possible once the saturation occurs. Hence,  $\mu$  could be fixed independently by information obtained in the pQCD calculation or in the deep inelastic scattering (DIS) through the relation to the saturation scale  $Q_s$  as a function

of  $\mu$ . [See a recent nice work [24] for careful discussions.] It is, of course, quite difficult to specify  $\mu$  for RHIC in this way because the relevant  $Q_s$  at RHIC is not unique from the kinematics unlike the DIS case.

The reason we would stick to rigorously also lies in the time scale of early evolution after the heavy-ion collision. A larger  $\mu$  may lift the underestimated energy and multiplicity up at the cost of changing the time scale  $\propto 1/\mu$ . Moreover, our finding must have a significant effect on the ‘‘Glasma’’ instability proposed in Ref. [25]. Because the correct treatment in the longitudinal direction is important in our argument, as we will see later, the instability with respect to the longitudinal variable (rapidity) should naturally be affected. Actually the instability is found too weak in Ref. [25]. It is likely that the numerical simulation in Ref. [25] underestimates the instability strength in the same way as for the energy density. If so, there might be a chance that the genuine Glasma instability would occur faster to contribute more or less to the early thermalization mechanism.

One more point that motivates us to reveal the discrepancy stemming from the numerical approximation is the infrared (IR) property of the MV model. The IR cutoff has a physical meaning, while the ultraviolet (UV) cutoff should be zero in the end. The dependence on the IR cutoff strongly relies on the approximation. This feature would bring about uncertainty, as is discussed in Ref. [24], in addition to the overall dimensionless factor.

In this work we will adopt the same prescription for the analytical calculations as in the numerical simulation to regularize the UV and IR singularities; we use the lattice formulation with the spacing and the system size given by  $a$  and  $La$ , respectively. This enables us to make a direct comparison between the analytical and numerical results.

## II. MCLERRAN-VENUGOPALAN MODEL

Here we will make a quick review on the MV model applied for the relativistic heavy-ion collision (two-source problem). If we have two sources which represent particles moving fast in the positive and negative  $z$ -directions (‘‘right’’ and ‘‘left’’ respectively), we can write the corresponding current using the light-cone coordinates as

$$J^\mu = \delta^{\mu+} \rho^{(1)}(\mathbf{x}_\perp, x^-) + \delta^{\mu-} \rho^{(2)}(\mathbf{x}_\perp, x^+), \quad (1)$$

where we dropped  $x^+$ -dependence in the right-moving source and  $x^-$ -dependence in the left-moving source as usual because of the Lorentz time dilatation. Then, converting the coordinates from the light-cone variables  $x^\pm$  to the proper-time  $\tau$  and the rapidity  $\eta$  which are related by  $x^\pm = (\tau/\sqrt{2})e^{\pm\eta}$ , we can express the initial fields right after two nuclei collide as [13, 23, 25]

$$\begin{aligned} E^\eta &= ig \left( [\alpha_1^{(1)}, \alpha_1^{(2)}] + [\alpha_2^{(1)}, \alpha_2^{(2)}] \right), \\ B^\eta &= ig \left( [\alpha_1^{(1)}, \alpha_2^{(2)}] + [\alpha_1^{(2)}, \alpha_2^{(1)}] \right), \end{aligned} \quad (2)$$

and the transverse fields ( $E^i$ ,  $B^i$ ) are zero [21], under the assumption that  $\rho^{(1)}(\mathbf{x}_\perp, x^-)$  and  $\rho^{(2)}(\mathbf{x}_\perp, x^+)$  behave like  $\delta(x^-)$  and  $\delta(x^+)$  respectively near the light cone [14]. This assumption is the case because of the Lorentz contraction when two nuclei travel at the speed of light. In the above, the color matrices,  $\alpha_i^{(n)}$ ’s, are the gauge field configurations in the radial gauge ( $A_\tau \propto x^- A^+ + x^+ A^- = 0$ ) created from each color source  $\rho^{(n)}$ . The solution must satisfy  $\partial_i \alpha_i^{(n)} = -\rho^{(n)}$  with a constraint that  $\alpha_i^{(n)}$  takes a pure gauge form so that its field strength is vanishing.

The covariant gauge is most convenient to get an explicit solution. By rotating the solution obtained in the covariant gauge to the radial gauge, we can write down the desirable solution as [6];

$$\alpha_i^{(1)}(\mathbf{x}_\perp, x^-) = -\frac{1}{ig} V(\mathbf{x}_\perp, x^-) \partial_i V^\dagger(\mathbf{x}_\perp, x^-), \quad \alpha_i^{(2)}(\mathbf{x}_\perp, x^+) = -\frac{1}{ig} W(\mathbf{x}_\perp, x^+) \partial_i W^\dagger(\mathbf{x}_\perp, x^+), \quad (3)$$

where the gauge rotation matrices are

$$\begin{aligned} V^\dagger(\mathbf{x}_\perp, x^-) &= \mathcal{P}_{x^-} \exp \left[ ig \int_{-\infty}^{x^-} dz^- \int d^2 \mathbf{y}_\perp G_0(\mathbf{x}_\perp - \mathbf{y}_\perp) \tilde{\rho}^{(1)}(\mathbf{y}_\perp, z^-) \right], \\ W^\dagger(\mathbf{x}_\perp, x^+) &= \mathcal{P}_{x^+} \exp \left[ ig \int_{-\infty}^{x^+} dz^+ \int d^2 \mathbf{y}_\perp G_0(\mathbf{x}_\perp - \mathbf{y}_\perp) \tilde{\rho}^{(2)}(\mathbf{y}_\perp, z^+) \right]. \end{aligned} \quad (4)$$

Here  $\mathcal{P}_{x^\pm}$  denotes the path-ordering with respect to  $x^\pm$ . We remark that  $\tilde{\rho}$  in Eq. (4) is the color source in the covariant gauge that is not identical to original  $\rho$  in the radial gauge. Since the Gaussian weight is a gauge-invariant function of  $\text{tr}[\rho^2] = \text{tr}[\tilde{\rho}^2]$  (see Eq. (7)), we do not have to discriminate  $\rho$  and  $\tilde{\rho}$  practically. We will thus not use

the tilde any more but just write  $\rho$  regardless of gauge. The two-dimensional massless propagator is defined by  $\partial_\perp^2 G_0(\mathbf{x}_\perp) = -\delta^{(2)}(\mathbf{x}_\perp)$  which is singular in both the IR and UV sectors. Let  $a$  and  $L$  be the lattice spacing and the number of the lattice sites, and then we can express  $G_0(\mathbf{x}_\perp)$  in the lattice regularization as

$$G_0(\mathbf{x}_\perp) = \frac{1}{2L^2} \sum_{n_i=1-L/2}^{L/2} \frac{\exp[i(x_1 2\pi n_1/La + x_2 2\pi n_2/La)]}{2 - \cos(2\pi n_1/L) - \cos(2\pi n_2/L)}. \quad (5)$$

The summation is supposed to exclude a singular point  $n_1 = n_2 = 0$  because we impose the global color neutrality  $\rho^{(n)}(\mathbf{p}_\perp = 0) = 0$ , so that the singular point  $n_1 = n_2 = 0$  does not appear at all in Eq. (4). It is easy to check that Eq. (5) is reduced to the standard expression,  $G_0(\mathbf{x}_\perp) \rightarrow \int d^2 \mathbf{p}_\perp e^{i\mathbf{x}_\perp \cdot \mathbf{p}_\perp} / [(2\pi)^2 \mathbf{p}_\perp^2]$ , in the continuum limit where  $a \rightarrow 0$  and  $L \rightarrow \infty$  are taken.

The later-time dynamics is uniquely determined by the equation of motion with the initial fields given by Eq. (2). Any physical observables are therefore given in terms of  $V$  and  $W$  in principle, which we shall denote as  $\mathcal{O}[V, W]$  generally. We can compute the expectation value by taking the average;

$$\langle \mathcal{O}[V, W] \rangle = \int [d\rho^{(1)}][d\rho^{(2)}] \mathcal{W}^{(1)}[\rho^{(1)}] \mathcal{W}^{(2)}[\rho^{(2)}] \mathcal{O}[V, W], \quad (6)$$

with the Gaussian weight,

$$\begin{aligned} \mathcal{W}^{(1)}[\rho^{(1)}] &= \exp \left[ - \int dx^- d^2 \mathbf{x}_\perp \frac{\text{tr}[\rho^{(1)}(\mathbf{x}_\perp, x^-)^2]}{g^2 [\mu^{(1)}(x^-)]^2} \right], \\ \mathcal{W}^{(2)}[\rho^{(2)}] &= \exp \left[ - \int dx^+ d^2 \mathbf{x}_\perp \frac{\text{tr}[\rho^{(2)}(\mathbf{x}_\perp, x^+)^2]}{g^2 [\mu^{(2)}(x^+)]^2} \right]. \end{aligned} \quad (7)$$

The normalization of the color trace is understood as  $\text{tr}[t^m t^n] = \frac{1}{2} \delta^{mn}$ , where  $t^m$ 's are the  $\text{SU}(N_c)$  algebra in the fundamental representation. The scale  $\mu^{(1)}(x^-)$  and thus  $\rho^{(1)}(\mathbf{x}_\perp, x^-)$  (or  $\mu^{(2)}(x^+)$  and thus  $\rho^{(2)}(\mathbf{x}_\perp, x^+)$ ) may have finite extent in the  $x^-$  (or  $x^+$  respectively) direction since the Lorentz  $\gamma$ -factor is finite in fact and also because the small- $x$  evolution by the JIMWLK equation should spread longitudinally in the color distribution.

If we are interested in evaluating the initial energy density in the heavy-ion collision,  $\mathcal{O}[V, W]$  should be  $\text{tr}[(E^\eta)^2 + (B^\eta)^2]$ , that is [17, 22],

$$\epsilon_0 = \langle \text{tr}[(E^\eta)^2 + (B^\eta)^2] \rangle = 2N_c(N_c^2 - 1) \langle \alpha^{(1)} \alpha^{(1)} \rangle \langle \alpha^{(2)} \alpha^{(2)} \rangle. \quad (8)$$

where we introduced a notation to indicate the diagonal component, i.e.  $\langle \alpha_i^a \alpha_j^b \rangle = \delta_{ij} \delta^{ab} \langle \alpha \alpha \rangle$  for  $\alpha^{(1)}$  and  $\alpha^{(2)}$  respectively. We will make use of this notation again when we show the numerical results later.

### III. QUESTION – NUMERICAL APPROXIMATION

In the numerical implementation, for practical reasons, it is difficult to compute the expectation value of the Wilson lines (4) as they are. In the first approximation the longitudinal finiteness is only negligible as compared to the transverse size and one can take the following limit;

$$\rho^{(1)}(\mathbf{x}_\perp, x^-) \rightarrow \bar{\rho}^{(1)}(\mathbf{x}_\perp) \delta(x^-), \quad \rho^{(2)}(\mathbf{x}_\perp, x^+) \rightarrow \bar{\rho}^{(2)}(\mathbf{x}_\perp) \delta(x^+). \quad (9)$$

Then one might anticipate that all physical quantities are given as a function of the integrated scale,

$$[\bar{\mu}^{(1)}]^2 = \int_{-\infty}^{\infty} dx^- [\mu^{(1)}(x^-)]^2, \quad [\bar{\mu}^{(2)}]^2 = \int_{-\infty}^{\infty} dx^+ [\mu^{(2)}(x^+)]^2. \quad (10)$$

As a matter of fact, we can verify this expectation in the analytical evaluation associated with only one source [8, 9, 12], that is, only  $[\bar{\mu}^{(1)}]^2$  (or  $[\bar{\mu}^{(2)}]^2$ ) appears in the Gaussian average of a function of  $V$  (or  $W$ ) with the weight  $\mathcal{W}^{(1)}[\rho^{(1)}]$  (or  $\mathcal{W}^{(2)}[\rho^{(2)}]$  respectively).

In the popular numerical formulation the Wilson lines (4) simplify approximately under the limit (9) as

$$\begin{aligned} V^\dagger(\mathbf{x}_\perp, x^-) &\stackrel{?}{\rightarrow} \bar{V}^\dagger(\mathbf{x}_\perp, x^-) = \exp \left[ ig \int d^2 \mathbf{y}_\perp G_0(\mathbf{x}_\perp - \mathbf{y}_\perp) \bar{\rho}^{(1)}(\mathbf{y}_\perp) \theta(x^-) \right], \\ W^\dagger(\mathbf{x}_\perp, x^+) &\stackrel{?}{\rightarrow} \bar{W}^\dagger(\mathbf{x}_\perp, x^+) = \exp \left[ ig \int d^2 \mathbf{y}_\perp G_0(\mathbf{x}_\perp - \mathbf{y}_\perp) \bar{\rho}^{(2)}(\mathbf{y}_\perp) \theta(x^+) \right]. \end{aligned} \quad (11)$$

These would be, of course, exact if there were not for the path-ordering  $\mathcal{P}_{x^\pm}$  or if in the Abelian gauge theory. The question we are addressing in the present paper is the validity of this naive prescription (11) that is commonly employed in the numerical simulation.

#### IV. MATHEMATICAL REPRESENTATION

Let us focus only on the  $V$ -sector in what follows because the initial energy density is factorized into the  $V$ -sector and the  $W$ -sector as is manifest in Eq. (8). Needless to say, exactly the same argument should work for the  $W$ -sector as well. For notational simplicity, then, we shall omit the superscript (1) which represents the right mover.

The subtle point comes from the fact that another Dirac delta function is involved implicitly in the formalism besides Eq. (9). Namely, the Gaussian weight (7) leads to the following correlation function;

$$\langle \rho_a(\mathbf{x}_\perp, x^-) \rho_b(\mathbf{y}_\perp, y^-) \rangle = g^2 [\mu(x^-)]^2 \delta^{ab} \delta(\mathbf{x}_\perp - \mathbf{y}_\perp) \delta(x^- - y^-). \quad (12)$$

We need to deal with two  $\delta(x^-)$ 's properly in order to formulate the problem in question in an appropriate way. For this goal it is convenient to introduce a regularization to the longitudinal Dirac delta functions. We modify the Wilson line accordingly as

$$V_\epsilon^\dagger(\mathbf{x}_\perp, x^-) = \mathcal{P}_{x^-} \exp \left[ ig \int_{-\infty}^{x^-} dz^- \int d^2 \mathbf{y}_\perp G_0(\mathbf{x}_\perp - \mathbf{y}_\perp) \rho_\epsilon(\mathbf{x}_\perp, z^-) \right], \quad (13)$$

where the regularized color source must be a smooth function satisfying

$$\lim_{\epsilon \rightarrow 0} \rho_\epsilon(\mathbf{x}_\perp, x^-) = \bar{\rho}(\mathbf{x}_\perp) \delta(x^-). \quad (14)$$

We shall introduce another regularization for the correlation function in a way as

$$\langle \rho_a(\mathbf{x}_\perp, x^-) \rho_b(\mathbf{y}_\perp, y^-) \rangle_\zeta = g^2 [\mu(x^-)]^2 \delta^{ab} \delta(\mathbf{x}_\perp - \mathbf{y}_\perp) \delta_\zeta(x^- - y^-), \quad (15)$$

such that the regularized delta function must satisfy

$$\lim_{\zeta \rightarrow 0} \delta_\zeta(z^-) = \delta(z^-). \quad (16)$$

We are now ready to elaborate the question in a mathematically sophisticated manner. The replacement of Eq. (11) is justified if  $\epsilon \rightarrow 0$  comes first before  $\zeta \rightarrow 0$ . In the analytical calculation, on the other hand, the relevant limit is  $\zeta \rightarrow 0$  followed by  $\epsilon \rightarrow 0$  later. Thus, a mathematically sensible description of the question (11) should be

$$\lim_{\zeta \rightarrow 0} \lim_{\epsilon \rightarrow 0} \langle \mathcal{O}[V_\epsilon] \rangle_\zeta \stackrel{?}{=} \lim_{\epsilon \rightarrow 0} \lim_{\zeta \rightarrow 0} \langle \mathcal{O}[V_\epsilon] \rangle_\zeta. \quad (17)$$

Here, the left-hand side corresponds to the numerical implementation (11) and the right-hand side corresponds to the one that is commonly assumed in the analytical works [8, 9, 10].

We sketch the intuitive interpretation of  $\epsilon$  and  $\zeta$  in Fig. 1. Roughly speaking,  $\epsilon$  is the longitudinal extent of a fast-moving nucleus and  $\zeta$  is the correlation length of the color distribution inside the nucleus. The physical limit should keep  $\epsilon > \zeta$  as is the case in the right-hand side of the question (17). If  $\epsilon$  goes to zero first, the longitudinal structure of randomness is lost. Then only one infinitesimal “sheet” of the two-dimensional random color distribution is left and the path-ordering becomes irrelevant (see also Fig. 4). The numerical prescription (11) hence implies such unphysical ordering of two noncommutative limits.

#### V. COMPARISON

We will explicitly confirm that the order of two limits is noncommutative indeed. We will begin with the simplest example of the tadpole expectation value. Then we will proceed to the case of the gauge fields which is directly related to the estimate for the initial energy density by Eq. (8). We note that the tadpole gives the scattering amplitude between a quark in the color fundamental representation and a CGC medium. This scattering amplitude is IR screened by long-ranged color interactions. In contrast to that, the gauge field correlation function involving four Wilson lines contains a color-singlet component which is free from screening. However, in this case, the derivative acting onto the

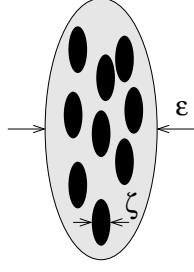


FIG. 1: Schematic picture of a nucleus with two regulators  $\epsilon$  and  $\zeta$ . Intuitively  $\epsilon$  signifies the longitudinal extent of the whole nucleus and  $\zeta$  stands for the longitudinal correlation length inside the nucleus. If randomness of the color source distribution is attributed to color confinement in each nucleon,  $\zeta$  corresponds to the longitudinal extent of the nucleon.

Wilson lines is UV harmful leading to singular behavior. It is possible to take the limit of vanishing UV cutoff ( $a \rightarrow 0$ ) at finite time ( $\tau \neq 0$ ) owing to non-linear evolution as has been closely investigated numerically in Refs. [21, 22] and analytically in Ref. [17]. The initial energy density in the heavy-ion collision at  $\tau = 0$  is, in this sense, an ill-defined quantity in the  $a \rightarrow 0$  limit. We will estimate it here, nevertheless, to compare the analytical and numerical outputs. It is partly because, whether it is a physical quantity or not, we are pursuing to exemplify a significant discrepancy anyhow. We will do this also partly because we know from Ref. [17] that the logarithmic singularity  $\sim [\ln(La/a)]^2$  at  $\tau = 0$  translates into  $\sim [\ln(La/\tau)]^2$  at  $\tau \neq 0$  with the overall coefficient unchanged. Thus, if we find a difference in the overall factor of the initial energy density as we will do below, the UV safe energy at  $\tau \neq 0$  should receive the same overall factor. Accordingly the initial energy estimate here could serve as correctness checking for UV safe observables indirectly.

### A. Tadpole

In the simplest case of the tadpole operator, i.e.  $\mathcal{O}[V] = V^\dagger$ , we can perform a quick comparison even without resorting to the numerical method. We already know the analytical answer for the right-hand side of Eq. (17). That is given by [9, 12]

$$\lim_{\epsilon \rightarrow 0} \lim_{\zeta \rightarrow 0} \langle V_\epsilon^\dagger \rangle_\zeta = \exp \left[ -g^4 \bar{\mu}^2 \frac{N_c^2 - 1}{4N_c} L(0, 0) \right], \quad (18)$$

where  $L(0, 0)$  is the notation in Ref. [9] which is defined as

$$L(0, 0) = \int d^2 \mathbf{x}_\perp G_0(\mathbf{x}_\perp) G_0(\mathbf{x}_\perp) = \frac{a^2}{4L^2} \sum_{n_i=1-L/2}^{L/2} \frac{1}{[2 - \cos(2\pi n_1/L) - \cos(2\pi n_2/L)]^2} \simeq \frac{0.962a^2}{2\pi} \left( \frac{L}{2\pi} \right)^2, \quad (19)$$

in the lattice regularization. Here, as in Eq. (5), the zero-mode ( $n_1 = n_2 = 0$ ) is to be removed by neutrality. The quadratic form approximates the sum quite well with a coefficient 0.962 that we find numerically.

As for the left-hand side of the question (17), we have to perform the following Gaussian integral;

$$\lim_{\zeta \rightarrow 0} \lim_{\epsilon \rightarrow 0} \langle V_\epsilon^\dagger \rangle_\zeta = \int [d\bar{\rho}] \exp \left[ ig \int d^2 \mathbf{y}_\perp G_0(\mathbf{x}_\perp - \mathbf{y}_\perp) \bar{\rho}(\mathbf{y}_\perp) \right] \exp \left[ - \int d^2 \mathbf{x}_\perp \frac{\text{tr}[\bar{\rho}(\mathbf{x}_\perp)^2]}{g^2 \bar{\mu}^2} \right]. \quad (20)$$

It should be mentioned that the first exponential part is a matrix, which makes the Gaussian integral hard to accomplish. Although it is a tough calculation for arbitrary  $SU(N_c)$  group, the  $SU(2)$  case ( $N_c = 2$ ) is feasible immediately because the  $SU(2)$  exponential matrix is easily manipulated. After some calculations we find that the above Gaussian integral results in

$$\lim_{\zeta \rightarrow 0} \lim_{\epsilon \rightarrow 0} \langle V_\epsilon^\dagger \rangle_\zeta = \left( 1 - g^4 \bar{\mu}^2 \frac{1}{4} L(0, 0) \right) \exp \left[ -g^4 \bar{\mu}^2 \frac{1}{8} L(0, 0) \right], \quad (21)$$

which obviously differs from Eq. (18) with  $N_c = 2$  substituted;

$$\lim_{\epsilon \rightarrow 0} \lim_{\zeta \rightarrow 0} \langle V_\epsilon^\dagger(\mathbf{x}_\perp) \rangle_\zeta = \exp \left[ -g^4 \bar{\mu}^2 \frac{3}{8} L(0, 0) \right]. \quad (22)$$

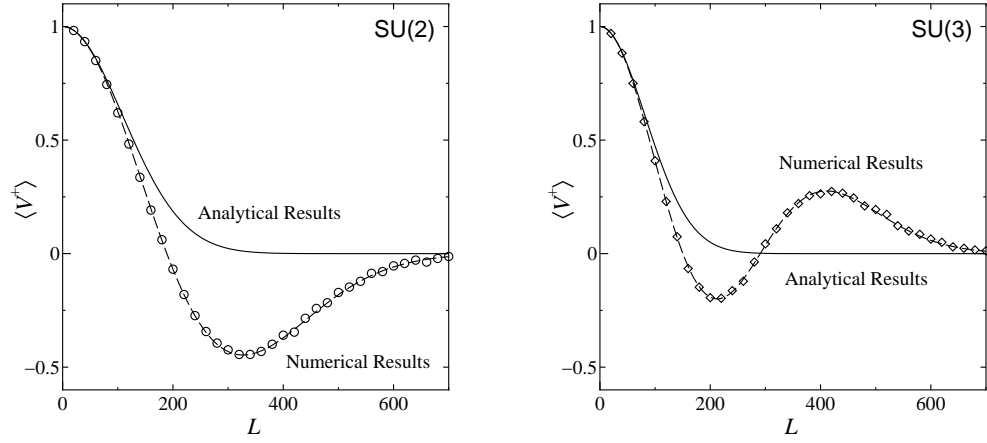


FIG. 2: Tadpole expectation value as a function of  $L$  with the parameter choice  $g^2\bar{\mu}a = 0.17$ . The left figure is for the SU(2) group and the right for the SU(3) group. The solid curves represent the analytical results by Eq. (18). The open circles represent the numerical results by the Monte-Carlo integration. The thin dashed curves show Eq. (21) in the SU(2) case and Eq. (25) in the SU(3) case, respectively. The SU(2) and SU(3) numerical data agree well with the thin dashed curves, which means that our Monte-Carlo integration works nicely.

It is interesting to see from the above that Eq. (21) can be a good approximation to Eq. (22) as long as  $g^2\bar{\mu}aL$  is small enough to allow for the Taylor expansion.

It should be instructive to compute Eq. (20) numerically in the Monte-Carlo integration though we already have the answer. In order to compare to the existing numerical calculations in literatures, we shall adopt the parameter choice same as used in Ref. [22]. That is,

$$\frac{g^2}{4\pi} = \frac{1}{\pi}, \quad g^2\bar{\mu}a = 0.17, \quad L = 700, \quad (23)$$

was chosen in Ref. [22] and then the nucleus size is given by

$$R_A = \frac{aL}{\sqrt{\pi}}. \quad (24)$$

We change the value of  $L$  to see the functional form. Therefore, if we increase  $L$  while keeping  $g^2\bar{\mu}a$  fixed at 0.17, the nucleus size or the infrared cutoff  $R_A$  grows up in proportion to  $L$ .

We plot the analytical formula (18) as a function of  $L$  by the solid curve for the SU(2) case in the left of Fig. 2 and the SU(3) case in the right of Fig. 2. Since  $g^2\bar{\mu}a$  is a constant, what Fig. 2 means is the  $R_A$ -dependence of the tadpole expectation value. The open circles in Fig. 2 represent the numerical results by means of the Monte-Carlo integration. We took 200 ensembles to calculate the expectation value. In the SU(2) case the numerical results agree well with the expression (21). Also, an analytical expression,

$$\lim_{\zeta \rightarrow 0} \lim_{\epsilon \rightarrow 0} \langle V_\epsilon^\dagger \rangle_\zeta = \left( 1 - g^4\bar{\mu}^2 \frac{1}{2} L(0,0) + g^8\bar{\mu}^4 \frac{1}{24} L(0,0)^2 \right) \exp \left[ -g^4\bar{\mu}^2 \frac{1}{6} L(0,0) \right], \quad (25)$$

can nicely fit the SU(3) results. In any case, it is obvious that the numerical results deviate from the analytical formula (18) substantially.

## B. Gauge Fields

In view of the tadpole results, one might have thought that the discrepancy is only minor. The deviation may look small, however, simply because the expectation value of color non-singlet operators is exponentially suppressed by the system size  $R_A$ . This fact becomes manifest once we consider some other operators that contain a color singlet component.

Here, let us elucidate a more complicated situation than the tadpole, that is, the expectation value of gauge fields  $\langle \alpha\alpha \rangle$  (see Eq. (8) for our notation) which have a contribution from the color singlet. In this case the Gaussian integral

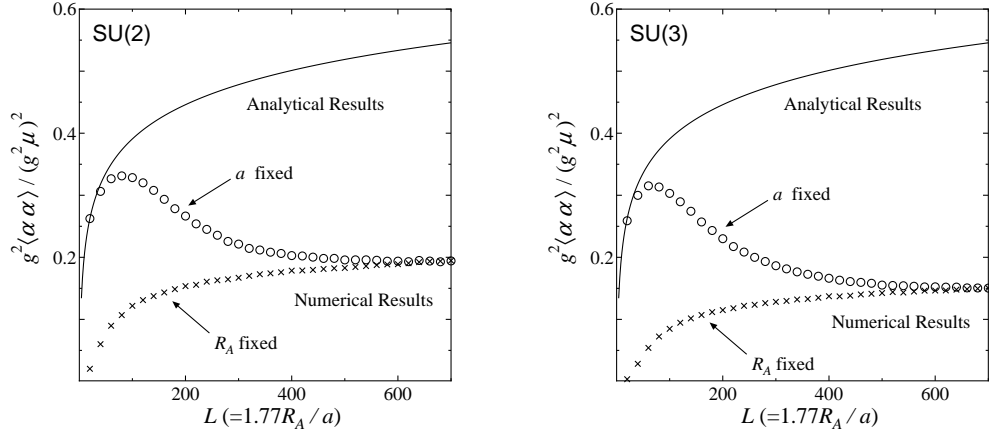


FIG. 3: Gauge field expectation value as a function of  $L$ . The analytical results are given by Eqs. (26) and (27). The parameter  $g^2\bar{\mu}a$  is fixed to be 0.17 for the  $a$ -fixed results and  $g^2\bar{\mu}a$  scales as  $0.17 \times 700/L$  for the  $R_A$ -fixed results. The left figure is for the SU(2) group and the right for the SU(3) group.

is too tedious to accomplish, so we will rely on the numerical Monte-Carlo integration only. On the other hand, the analytical calculation with the path-ordering is still possible and it follows;

$$\langle\alpha\alpha\rangle = \frac{1}{g^2}(g^2\bar{\mu})^2 \sigma, \quad (26)$$

where

$$\sigma = \frac{1}{4L^2} \sum_{n_i=1-L/2}^{L/2} \frac{1}{2 - \cos(2\pi n_1/L) - \cos(2\pi n_2/L)} \simeq \frac{1}{4\pi} \ln(1.36L) = \frac{1}{4} \ln(2.41R_A/a), \quad (27)$$

which does not depend on  $N_c$  at all and monotonically grows up with increasing  $L$ . We numerically find a constant 1.36 in the logarithm which approximates the sum. This expression is, hence, both IR and UV singular. That is,  $\langle\alpha\alpha\rangle \rightarrow \infty$  whenever  $L \rightarrow \infty$  (i.e. either  $R_A \rightarrow \infty$  with  $a$  fixed or  $a \rightarrow 0$  with  $R_A$  fixed, see Eq. (24)). More importantly, the analytical formulae (26) and (27) claim that the IR behavior as  $R_A \rightarrow \infty$  and the UV behavior as  $a \rightarrow 0$  are completely identical. This property is, however, no longer the case in the numerical results with wrong approximation assumed, which could be a possible explanation for IR stability found in Ref. [18].

Figure 3 shows the results by the Monte-Carlo integration. The shape of  $g^2\langle\alpha\alpha\rangle/(g^2\bar{\mu})^2$  as a function of  $L$  clearly depends on whether  $R_A \propto L$  increases with  $a$  fixed or  $a \propto 1/L$  decreases with  $R_A$  fixed. In the case that  $a$  is fixed, the calculation goes just in the same way as in the previous subsection; we choose  $g^2\bar{\mu}a = 0.17$ . When we keep  $R_A$  fixed, we adjust the lattice spacing as  $g^2\bar{\mu}a = 0.17 \times 700/L$ , so that  $g^2\bar{\mu}a$  becomes 0.17 for  $L = 700$ , which is completely equivalent to the procedure in Ref. [22]. Thus, the  $a$ -fixed curve and  $R_A$ -fixed curve should meet at  $L = 700$ , as is certainly the case in Fig. 3.

The numerical results hardly depend on  $N_c$ ; the left and right figures of Fig. 3 look almost the same, though the SU(3) results are slightly smaller than the SU(2) ones. The numerical calculation leads to  $g^2\langle\alpha\alpha\rangle/(g^2\bar{\mu})^2 = 0.194$  at  $L = 700$  for the SU(2) group, while the SU(3) group results in 0.150 at  $L = 700$ . Differently from the tadpole case, the numerical data underestimate the expectation value that is  $g^2\langle\alpha\alpha\rangle/(g^2\bar{\mu})^2 = \sigma = 0.546$  in the analytical method. In the next section, we will discuss how we may be able to remedy this situation.

## VI. IMPROVEMENT

We can improve the situation by inserting the infinitesimal sheet in longitudinal extent in a way as sketched in Fig. 4. We denote the number of sheets by  $N_\eta$ . We note that  $N_\eta$  is *not* the longitudinal coordinate as in Ref. [25], but it is the number of slices within infinitesimal extent. Hence, all the numerical results we have seen so far correspond to  $N_\eta = 1$ . We can recover the full path-ordering in the  $N_\eta \rightarrow \infty$  limit.

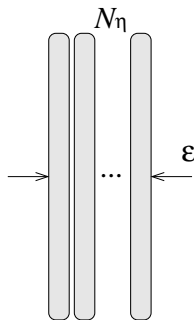


FIG. 4: Schematic picture of how to improve the numerical results. Each blob represents the two-dimensional sheet without longitudinal randomness. In the  $N_\eta \rightarrow \infty$  limit we can recover the full randomness structure in longitudinal extent which is infinitesimal in the  $\epsilon \rightarrow 0$  limit.

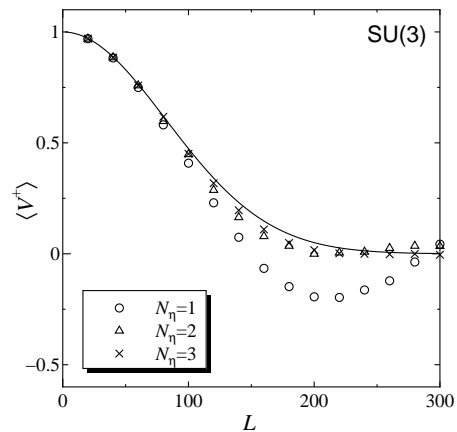


FIG. 5: Tadpole expectation value for the SU(3) case at  $N_\eta = 1$  (same as shown previously),  $N_\eta = 2$ , and  $N_\eta = 3$ .

For example, in the tadpole case, we shall modify the Gaussian integral in Eq. (20) into the form of

$$\langle V^\dagger \rangle_{N_\eta} = \prod_{n=1}^{N_\eta} \int [d\bar{\rho}_n] \exp \left[ ig \int d^2 \mathbf{y}_\perp G_0(\mathbf{x}_\perp - \mathbf{y}_\perp) \bar{\rho}_n(\mathbf{y}_\perp) \right] \exp \left[ - \int d^2 \mathbf{x}_\perp \frac{\text{tr}[\bar{\rho}_n(\mathbf{x}_\perp)^2]}{g^2(\bar{\mu}^2/N_\eta)} \right], \quad (28)$$

to retrieve the analytical results in the limit of  $N_\eta \rightarrow \infty$ . We have to divide  $\bar{\mu}^2$  by  $N_\eta$  to make it consistent with Eq. (10). It is, however, impossible to take the  $N_\eta \rightarrow \infty$  limit in the practical procedure. Instead, in this section let us focus only on  $N_\eta = 2$ ,  $N_\eta = 3$ , and  $N_\eta = 10$  to demonstrate the tendency of how the numerical outputs could move from the structureless  $N_\eta = 1$  results toward the analytical answer. We did calculate in the SU(2) case as well as in the SU(3) case, but we will present only the SU(3) results here, for the gauge group makes no qualitative difference.

The improvement works nicely for the tadpole expectation value as is evident in Fig. 5. The results at  $N_\eta = 2$  almost reproduces the analytical curve. So, the strategy to cure the pathology might seem promising.

However, the gauge field expectation value scarcely benefits from this improvement procedure. We show the results in Fig. 6 for the  $a$ -fixed calculation (left) and the  $R_A$ -fixed calculation (right). The improvement seems rather better for the IR behavior with  $a$  fixed. The UV behavior with  $R_A$  fixed barely moves with increasing  $N_\eta$ . This is because the reference point for the  $R_A$ -fixed calculation is chosen at  $L = 700$  where the deviation between the analytical and numerical results is acute as perceived from Fig. 3. So,  $N_\tau$  must be comparable to  $\sim 700$  to achieve a nice deal of improvement for the  $R_A$ -fixed results. We would observe better convergence if  $g^2 \bar{\mu} a L$  is smaller than  $0.17 \times 700$  that we chose here.

## VII. DISCUSSIONS – FROM A “MODEL” TO A “THEORY”

From the comparison between the analytical and numerical outputs, we can learn an important lesson; the numerical implementation like Eq. (11) needs more and more caution as we approach the continuum limit in the transverse plane. This is a sort of dilemma. We should insert more and more sheets along the longitudinal direction as in Fig. 4 when we want to make use of a finer lattice or a larger volume in the simulation. Of course, the computation time increases as  $N_\eta$  gets larger because the number of the integration variables is proportional to  $N_\eta$  as seen in Eq. (28).

We shall apply our results to the comparison of the initial energy density between the analytical formula by Eq. (8) and what was reported in Ref. [22]. As we have discussed, the numerical formulation with the approximation (11) underestimates the gauge field expectation value by a factor  $0.546/0.15 = 3.64$ . Therefore, the initial energy density obtained in the numerical method is smaller than the analytical estimate by a factor  $3.64^2 = 13.2$ .

We plot the initial energy density in Fig. 7. It should be mentioned that, though the important message from Ref. [22] is that the initial energy density at  $\tau = 0$  is ill-defined and logarithmically divergent in the  $R_A \rightarrow \infty$  limit, our analytical calculation ends up with a finite value with the IR and UV cutoffs (i.e.  $a > 0$  and  $L < \infty$ ), which is just the same as the lattice discretized results.



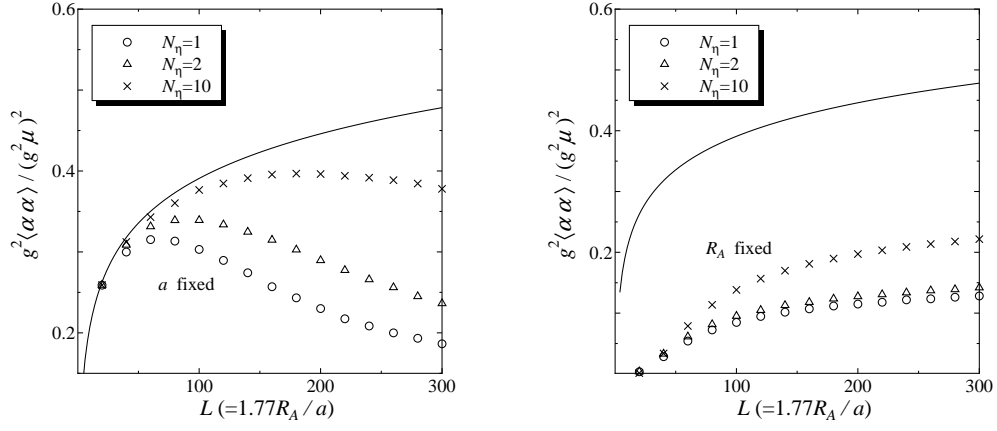


FIG. 6: Gauge field expectation value for the SU(3) case at  $N_\eta = 1$  (same as shown previously),  $N_\eta = 2$ , and  $N_\eta = 10$ . The convergence to the analytical answer is much slower than the tadpole case especially for larger  $L$ .

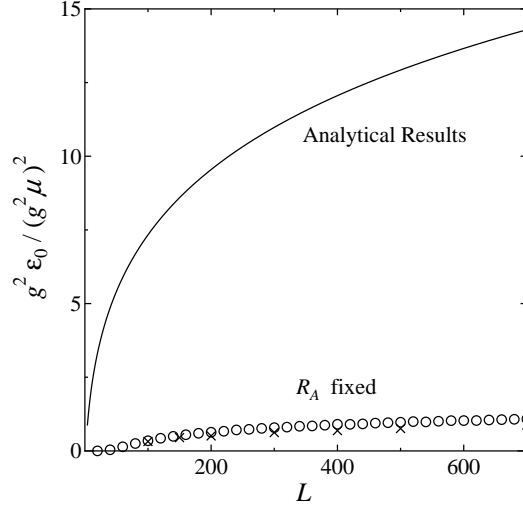


FIG. 7: Initial energy density in the analytical calculation shown by the solid curve and the numerical estimate shown by the open circles. The cross points represent the data presented in Ref. [22].

It is notable that our numerical estimate is close to the data calculated in the numerical simulation in Ref. [22] which is overlaid on Fig. 7 by the cross points. The small discrepancy should be explained by difference between the naive discretization in this work and the gauge-invariant lattice formulation in terms of the link variables.

One should not jump to a conclusion, however, that the initial energy density becomes 13.2 times larger than the estimate in the previous numerical works. To earn a right interpretation, we have to understand how to specify the MV model parameter  $\bar{\mu}$ . The determination of  $\bar{\mu}$  has been carefully explained in the pioneering works [18, 20] and their choice ( $g = 2$  and  $g^2\bar{\mu} = 2$  GeV for RHIC) has become a standard. Section V A in Ref. [20] is actually devoted to elaborating that  $\bar{\mu} = 0.5$  GeV can reproduce the total multiplicity at RHIC and then the following energy density is in a reasonable range. This procedure would make the discrepancy between the analytical and numerical results hidden behind the fitting; not only the energy density but also the multiplicity is accompanied by the factor 3.64. [The multiplicity is an integration over the gauge field expectation value divided by the particle dispersion relation.] That means that the value of  $\bar{\mu}$  would become  $\sqrt{3.64} = 1.9$  times larger in order to fit the total multiplicity without the overall factor 3.64, leading to  $3.64^2 = 13.2$  times larger energy density. Consequently, even though the dimensionless coefficient has a substantial factor, the dimensional quantity *in the physical unit* remains unchanged. In other words the saturation model has only one dimensional scale  $\bar{\mu}$  and all the physical quantities are expected to scale with  $\bar{\mu}$ . Once  $\bar{\mu}$  is fixed by means of one of the experimental data set, other observables from the model calculation should be all consistent with the whole data set.

Then, one might be confused at what the point of our finding is in this work. Our aim is, as emphasized in

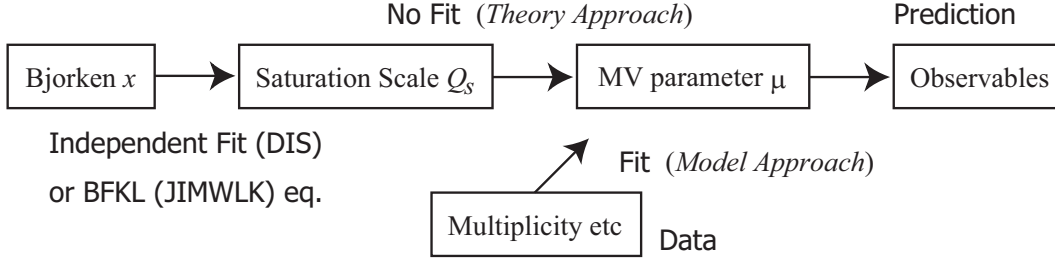


FIG. 8: Schematic chart for the theory and model approaches.

Introduction, to establish a correct *theoretical* procedure for the MV model. For that purpose the phenomenological success is inadequate. We must treat the MV model scale  $\bar{\mu}$  not as a fitting parameter but as an input deduced theoretically from a given Bjorken's  $x$ . This is, in principle, possible with the BFKL equation from which the saturation scale  $Q_s$  is inferred as a function of  $x$ . [The nonlinear extension of the BFKL equation, namely the JIMWLK equation, is not necessary for the determination of  $Q_s(x)$  as concisely explained in Ref. [26].] The theoretical uncertainty by higher order corrections is still large, however, and the Golec-Biernat-Wüsthof fit multiplied by the atomic number factor  $A^{1/3}$  is usually regarded as a more trustworthy form of  $Q_s(x)$ . Then, within the framework of the MV model, the saturation scale can be defined in terms of  $\bar{\mu}$  as

$$Q_s^2 \simeq \frac{N_c g^2 \bar{\mu}^2}{4\pi} \ln(Q_s^2/\Lambda^2), \quad (29)$$

where  $\Lambda$  is the IR cutoff. That is,  $\Lambda$  is given by  $R_A$  in the present work, while it should be the confinement scale  $\sim 1$  fm in reality. We can specify  $\bar{\mu}$  corresponding to relevant  $x$  through  $Q_s(x)$  using Eq. (29).

We would call the above-mentioned strategy as the theory approach in contrast to the model approach where  $\bar{\mu}$  is phenomenologically fixed by the total multiplicity. Our point of view is summarized as a chart in Fig. 8. This present work is a first-step attempt to complete the full theory approach.

Our finding that the longitudinal structure in infinitesimal extent has a significant effect may well be important also for the instability analyses in Ref. [25], as we already mentioned in Introduction. Because the instability takes place with respect to the longitudinal fluctuations, it is naturally expected that the proper treatment of longitudinal randomness should alter the quantitative features discussed in Ref. [25]. It is an intriguing question whether the instability would remain weak as concluded in Ref. [25] or not with longitudinal randomness taken into account. If not, the instability might be fast and strong enough to account for the early thermalization. We have to emphasize that our  $N_\eta$  is not the same as  $L_\eta$  employed in Ref. [25] in which the authors introduced the longitudinal *coordinate* to solve the equation of motion in three-dimensional space, but did not store the random sheets within infinitesimal extent *in the initial condition*. The vital difference lies in the fact that the number of the Monte-Carlo integration variables  $\bar{\rho}_n(\mathbf{x}_\perp)$  ( $n = 1, \dots, N_\eta$ ) becomes greater with increasing  $N_\eta$ . We conjecture that the Glasma instability would become stronger with  $N_\eta > 1$ , but the quantitative analyses have to wait for at least  $N_\eta$  times expensive computations as compared to Ref. [25], which is the problem to be investigated in the future.

### Acknowledgments

The author thanks Teiji Kunihiro for useful conversations, Paul Romatschke for encouraging and helpful comments, and Raju Venugopalan for communications.

- 
- [1] L. D. McLerran and R. Venugopalan, Phys. Rev. D **49**, 2233 (1994) [arXiv:hep-ph/9309289]; 3352 (1994) [arXiv:hep-ph/9311205]; D **50**, 2225 (1994) [arXiv:hep-ph/9402335].
  - [2] For reviews, see: E. Iancu and R. Venugopalan, arXiv:hep-ph/0303204; E. Iancu, A. Leonidov and L. McLerran, arXiv:hep-ph/0202270.
  - [3] L. V. Gribov, E. M. Levin and M. G. Ryskin, Phys. Rept. **100**, 1 (1983).
  - [4] A. M. Stasto, K. J. Golec-Biernat and J. Kwiecinski, Phys. Rev. Lett. **86**, 596 (2001) [arXiv:hep-ph/0007192].
  - [5] E. Iancu, K. Itakura and L. McLerran, Nucl. Phys. A **724**, 181 (2003) [arXiv:hep-ph/0212123].
  - [6] Y. V. Kovchegov, Phys. Rev. D **54**, 5463 (1996) [arXiv:hep-ph/9605446].

- [7] J. Jalilian-Marian, A. Kovner, L. D. McLerran and H. Weigert, Phys. Rev. D **55**, 5414 (1997) [arXiv:hep-ph/9606337].
- [8] J. P. Blaizot, F. Gelis and R. Venugopalan, Nucl. Phys. A **743**, 13 (2004) [arXiv:hep-ph/0402256].
- [9] J. P. Blaizot, F. Gelis and R. Venugopalan, Nucl. Phys. A **743**, 57 (2004) [arXiv:hep-ph/0402257].
- [10] F. Gelis and Y. Mehtar-Tani, Phys. Rev. D **73**, 034019 (2006) [arXiv:hep-ph/0512079].
- [11] Y. Hatta, Nucl. Phys. A **781**, 104 (2007) [arXiv:hep-ph/0607126].
- [12] K. Fukushima and Y. Hidaka, JHEP **0706**, 040 (2007) [arXiv:0704.2806 [hep-ph]].
- [13] A. Kovner, L. D. McLerran and H. Weigert, Phys. Rev. D **52**, 3809 (1995) [arXiv:hep-ph/9505320]; 6231 (1995) [arXiv:hep-ph/9502289].
- [14] M. Gyulassy and L. D. McLerran, Phys. Rev. C **56**, 2219 (1997) [arXiv:nucl-th/9704034].
- [15] Y. V. Kovchegov and D. H. Rischke, Phys. Rev. C **56**, 1084 (1997) [arXiv:hep-ph/9704201].
- [16] R. J. Fries, J. I. Kapusta and Y. Li, arXiv:nucl-th/0604054.
- [17] K. Fukushima, Phys. Rev. C **76**, 021902 (2007) [arXiv:0704.3625 [hep-ph]].
- [18] A. Krasnitz and R. Venugopalan, Nucl. Phys. B **557**, 237 (1999) [arXiv:hep-ph/9809433]; Phys. Rev. Lett. **84**, 4309 (2000) [arXiv:hep-ph/9909203]; **86**, 1717 (2001) [arXiv:hep-ph/0007108].
- [19] A. Krasnitz, Y. Nara and R. Venugopalan, Phys. Rev. Lett. **87**, 192302 (2001) [arXiv:hep-ph/0108092]; Nucl. Phys. A **717**, 268 (2003) [arXiv:hep-ph/0209269]; **727**, 427 (2003) [arXiv:hep-ph/0305112].
- [20] T. Lappi, Phys. Rev. C **67**, 054903 (2003) [arXiv:hep-ph/0303076].
- [21] T. Lappi and L. McLerran, Nucl. Phys. A **772**, 200 (2006) [arXiv:hep-ph/0602189].
- [22] T. Lappi, Phys. Lett. B **643**, 11 (2006) [arXiv:hep-ph/0606207].
- [23] K. Fukushima, F. Gelis and L. McLerran, Nucl. Phys. A **786**, 107 (2007) [arXiv:hep-ph/0610416].
- [24] T. Lappi, arXiv:0711.3039 [hep-ph].
- [25] P. Romatschke and R. Venugopalan, Phys. Rev. Lett. **96**, 062302 (2006) [arXiv:hep-ph/0510121]; Phys. Rev. D **74**, 045011 (2006) [arXiv:hep-ph/0605045].
- [26] D. Kharzeev, E. Levin and M. Nardi, Nucl. Phys. A **747**, 609 (2005) [arXiv:hep-ph/0408050].